Plastron Induced Drag Reduction and Increased Slip on a Superhydrophobic Sphere

Glen McHale*, Morris R. Flynn and Michael I. Newton

Notable drag reduction can occur when a superhydrophobic object immersed in a flowing liquid contains a surface-retained film of air (a plastron).

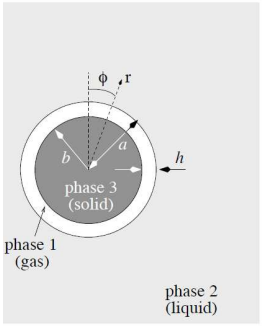

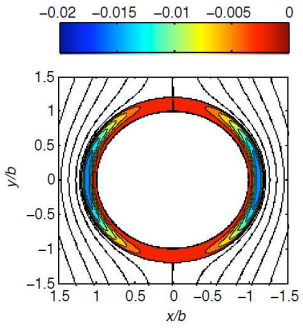

Plastron Induced Drag Reduction and Increased Slip on a Superhydrophobic Sphere

G. McHale[1$], M.R. Flynn[#] and M. I. Newton[$]

[$]*School of Science and Technology, Nottingham Trent University,*

Clifton Lane, Nottingham NG11 8NS, UK.

[#]*Department of Mechanical Engineering, University of Alberta,*

Edmonton, AB T6G 2G8, Canada.

Abstract

On low contact angle hysteresis superhydrophobic surfaces, droplets of water roll easily. It is intuitively appealing, but less obvious, that when such material is immersed in water, the liquid will flow more easily across its surface. In recent experiments it has been demonstrated that superhydrophobic surfaces with the same high contact angle and low contact angle hysteresis may not, in fact, have the same drag reducing properties. A key performance parameter is whether the surface is able to retain a layer of air (i.e. a plastron) when fully immersed. In this report, we consider an analytical model of Stokes flow (i.e. low Reynolds number, *Re*, creeping flow) across a surface retaining a continuous layer of air. The system is based on a compound droplet model consisting of a solid sphere encased in a sheathing layer of air and is the extreme limit of a solid sphere with a superhydrophobic surface. We demonstrate that an optimum thickness of air exists at which the drag on this compound object is minimized and that the level of drag reduction can approach 20 to 30%. Physically, drag reduction is caused by the ability of the external flow to transfer momentum across the water-air interface generating an internal circulation of air within the plastron. We also show that the drag experienced by the plastron-retaining sphere can be viewed as equivalent to the drag on a non-plastron retaining sphere, but with the no-slip boundary condition replaced by a slip boundary condition. If the plastron layer becomes too thin, or the liquid-gas interface is rigidified, circulation is no longer possible and drag increases to the value expected for a solid object in direct contact with water. We discuss the implications of this physical understanding in terms of its general applicability to the intelligent design of drag reducing superhydrophobic surfaces at low *Re*. We emphasize that the length scales and connectivity of surface topography generating superhydrophobicity are also likely to determine whether a plastron is of a suitable size to reduce drag.

Keywords: Superhydrophobic, slip, drag, plastron, contact angle, wetting.

[1] Corresponding author: glen.mchale@ntu.ac.uk
Tel: +44 (0)115 8483383

1. Introduction

In recent years there has been increasing interest in the use of topography to amplify the effects of hydrophobic surface chemistry to create superhydrophobic surfaces.[1] Methods for creating such surfaces with both nano-scale and micro-scale features are well developed[2] and this has allowed studies to be extended to include possible effects beyond simple non-wetting properties. One area of significant focus has been the behaviour of superhydrophobic surfaces when fully immersed in water.[3] It has long been recognized by arthropod physiologists, that the silvery reflections observed from some aquatic insects and spiders are caused by thin films of air retained underwater by natural (superhydrophobic) morphological adaptations to their bodies.[4-6] Within the natural world, plastrons enable oxygen and carbon dioxide exchange between these arthropods and water thereby enabling underwater respiration without the need for gills. An advantage of plastron respiration compared to bubble respiration is that the pinning of the air-liquid interface by rigid hydrophobic hairs stabilizes the layer of gas and effectively stiffens the gas bubble.[7] In the modern era of superhydrophobicity, the ability of superhydrophobic materials to perform the same function as an arthropod plastron was first demonstrated, by several of the current authors, using a superhydrophobic sol-gel foam[8] with complementary calculations presented in Flynn and Bush.[9]

One property of superhydrophobic surfaces with large advancing contact angle and low contact angle hysteresis is their ability to shed droplets of water with ease; so-called slippy superhydrophobic surfaces. This has led to consideration of whether superhydrophobic surfaces can reduce the drag of liquids flowing across them,[10,11] although it is not obvious whether low contact angle hysteresis (i.e. whether a surface is slippy or sticky[12]) would be an important factor. Experiments on drag reduction, or equivalently large slip lengths, have used a range of different experimental approaches including micro-particle image velocimetry and pressure drop measurements,[13,14] hydrofoil measurements,[15] cone-and-plate rheometers,[16] pressure drop and flow-rate measurements,[17] and quartz crystal microbalance resonators.[18-20] Most of these methods involve a fixed surface subject to a flow. [#]

Recently, two of the current authors described an alternative approach involving the settling of a sphere with a superhydrophobic coating in a large cylinder of water.[21] In the experiments reported, a method, inspired by the insect physiology literature, of comparing the same sphere with and without a plastron was developed using an ethanol pre-wetting out procedure. It was suggested in that work that a key feature of the reduction in drag was the ability of a plastron to support an internal circulation of air thus implying that a minimum thickness plastron was required for a superhydrophobic surface to display drag reduction or apparent slip. The possible relevance of this viewpoint to both laminar and turbulent flow regimes was discussed in a recent article.[3] Most recently, a similar terminal velocity of a settling sphere experiment has been reported, but using heat to generate a uniform encapsulating layer of vapour *via* the Leidenfrost effect, and this showed drag reduction of over 85% in the sub-critical transition to a turbulent flow regime.[22]

To assist in the interpretation of experimental results, and also add some physical context to the use of plastrons for drag reduction rather than respiration in the natural world[23], we theoretically investigate a model of drag on a solid spherical object possessing a surface-retained

[#] Note added to postprint: See also P. Muralidhar, N. Ferrer, R. Daniello and J.P. Rothstein, *J. Fluid Mech*. **2011**, *680*, 459-476.

layer of air (a plastron) in the low Reynolds number (creeping flow) regime. The plastron in this idealized model is of uniform thickness; as such, we consider the limit of a solid sphere with a perfect superhydrophobic surface. In flow past a gas bubble or droplet attached to a wall, flow can result in deformations of the bubble or droplet surface[24] and contribute to drag. However, because the air layer within a plastron is supported by a rigid hydrophobic surface structure it is a reasonable assumption that the layer is of uniform and constant thickness independent of the precise details of the external flow. (Formally this requires capillary forces to dominate shear forces so that, in the absence of fluid inertia, the capillary number, *Ca*, is less than approximately 0.5.[25]) Note, moreover, that distortions and ripples of the gas-liquid interface are less likely to contribute significantly to drag at low Reynolds numbers.

From our model, we show that there is an optimum plastron thickness for drag reduction: the plastron must be thick enough to allow for internal air circulation but thin enough that the additional cross-section of the compound object (i.e. solid plus plastron) does not become too large. We derive a relationship between drag reduction and an apparent slip length and investigate their relationship with the thickness of the plastron. Moreover, we show that in a terminal velocity experiment, the reduction in drag caused by a plastron can be sufficiently large that it overcomes the additional buoyancy created by the air contained within the plastron – a plastron-retaining sphere can fall faster than one not encased by a layer of air. We discuss the relevance of these results to real systems by addressing the design of drag-reducing superhydrophobic surfaces. Finally, we consider a particular example from nature where the plastron function is associated specifically with drag reduction.

2. Theoretical Approach

2.1 Fluid Mechanics Formulation

The defining equations of fluid mechanics are reviewed below so that all assumptions are stated explicitly. In the small Reynolds number limit describing creeping flow (i.e. $Re \ll 1$), the Navier-Stokes equations of motion reduce to,[26]

$$\underline{\nabla} p = \eta \nabla^2 \underline{u} \qquad (1)$$

where $\underline{u}$ and p are the local fluid velocity and pressure and η is the viscosity. Any solution for the fluid velocity must also satisfy the continuity equation,

$$\underline{\nabla}.\underline{u} = 0 \qquad (2)$$

Axisymmetric flows for which dependent variables are independent of the azimuthal angle φ can be examined by introducing a streamfunction, $\psi(r,\theta)$, where r and θ denote, respectively, the radial distance and polar angle. Thus the non-zero radial and angular components of fluid velocity, u_r and u_θ, can be written as,

$$u_r(r,\theta) = -\frac{1}{r^2 \sin\theta}\frac{\partial \psi(r,\theta)}{\partial \theta} \quad \text{and} \quad u_\theta(r,\theta) = \frac{1}{r \sin\theta}\frac{\partial \psi(r,\theta)}{\partial r} \qquad (3)$$

respectively. For the streamfunction to be a solution of the equation of motion, Eq. (1), it must satisfy the equation,

$$\left[\frac{\partial^2}{\partial r^2}+\frac{\sin\theta}{r^2}\frac{\partial}{\partial\theta}\left(\frac{1}{\sin\theta}\frac{\partial}{\partial\theta}\right)\right]^2\psi(r,\theta)=0 \qquad (4)$$

Trial solutions to Eq. (4) of the form $r^n\sin^2\theta$, show that n=-1, 1, 2, and 4 are possible so that the general solution is of the form,[27]

$$\psi(r,\theta)=\sin^2\theta\left[\frac{1}{10}Ar^4-\frac{1}{2}Br+Cr^2+\frac{D}{r}\right] \qquad (5)$$

This general solution can be made specific to a given situation by applying boundary conditions. For flow around an obstacle, one of the boundary conditions is that the radial and tangential components of velocity must tend to the free stream velocity, U_∞, at large r, i.e.

$$u_r(r,\theta)\to -U_\infty\cos\theta \qquad \text{and} \qquad u_\theta(r,\theta)\to U_\infty\sin\theta \qquad (6)$$

2.2 Encapsulated Droplet Solution

Our interest is in the difference in flow and consequent drag force that occurs when a solid spherical object of radius, b, is enveloped in a persistent, concentric spherical shell of sheathing air. This problem, illustrated schematically in fig. 1, is a special case of a three-phase system in which a compound droplet consisting of a core fluid (phase 3) enveloped by a sheathing fluid (phase 1) of radius $a=b/\varepsilon$, where $\varepsilon<1$, moves through an external medium (phase 2). In this general case, there is a streamfunction, defined by Eq. (5), for each of the three phases. Rushton and Davies[27] considered this problem in 1983 and matched the boundary conditions requiring the velocity components to remain finite (including at r=0), the velocity and tangential stresses to be continuous at the boundaries between adjacent phases and the normal velocity components to vanish at the boundaries (so that phases do not mix).[28] Their solution for the frictional drag force, F_d^c, on the compound fluid object reads,

$$F_d^c=\frac{2}{3}\left[\frac{\eta_{32}+6\eta_{12}^2G(\varepsilon)+\eta_{12}(2+3\eta_{32})F(\varepsilon)}{\eta_{32}+4\eta_{12}^2G(\varepsilon)+2\eta_{12}(1+\eta_{32})F(\varepsilon)}\right]F_d^{St}(a) \qquad (7)$$

where $F_d^{St}(a)=-6\pi\eta_2aU_\infty$ is the Stokes drag force on a solid sphere of radius a, $\eta_{ij}=\eta_i/\eta_j$ and the functions $F(\varepsilon)$ and $G(\varepsilon)$ are defined by,

$$F(\varepsilon)=\frac{(1+\varepsilon)(2\varepsilon^2+\varepsilon+2)}{(1-\varepsilon)(4\varepsilon^2+7\varepsilon+4)} \qquad \text{and} \qquad G(\varepsilon)=\frac{(1-\varepsilon^5)}{(1-\varepsilon)^3(4\varepsilon^2+7\varepsilon+4)} \qquad (8)$$

The corresponding streamfunctions were not given in Rushton and Davies's study, but were reported in the related investigation of Ferreira *et al.*[29] The general solutions are algebraically intricate and are reproduced in the supplementary information (Appendix A) for completeness, where we also consider the limiting case $\eta_{32}\to\infty$, pertinent to a compound droplet with a solid core (Eqs. A6-A8).

Rushton and Davies[27] discussed the limits of the frictional drag force and showed that a sphere of a single fluid of radius a (i.e. $\varepsilon\to0$) has a drag correction compared to Stokes' law of $\lambda_{HR}=(2/3)(1+3\eta_{12}/2)/(1+\eta_{12})$, which is the Hadamard-Rybczinski result;[30-32] for a bubble of air in water, η_{12} is small (i.e. less than about 0.02), and thus to a very good approximation $\lambda_{HR}\approx2/3$.

Rushton and Davies[27] also showed that if the encapsulating phase 1 fluid is extremely thin (i.e. $\varepsilon \to 1$) the compound fluid experiences the same drag force as a solid particle of radius a, despite the core being a fluid. The source of this (possibly surprising) result is that the circulation of fluid in the encapsulating fluid shell becomes suppressed and so the phase 1 fluid becomes immobile and unable to transfer momentum across the boundary into the encapsulated fluid (phase 3). This is an equivalent effect to the adsorption of surfactants or impurities on a bubble rigidifying the gas-liquid interface and so rendering the interface immobile.[28,33] Rigidifying the gas-liquid interface prevents momentum transfer and results in higher drag equal to that predicted by Stokes' law.[34]

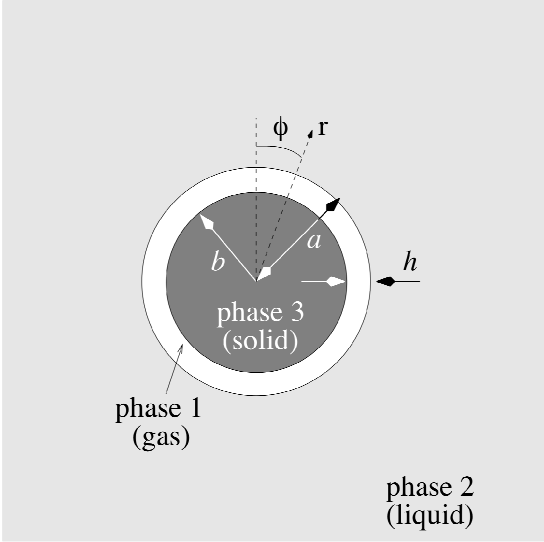

Figure 1. Schematic of a plastron-bearing solid sphere in a liquid ambient.

3. Results for Plastron-Bearing Superhydrophobic Sphere

3.1 Drag Formula

To assess the effect of a plastron of thickness h, on a solid sphere of radius b, we modify the above notation by writing η_g, η_l and $\eta_s \to \infty$, respectively, in place of η_1, η_2 and η_3. Next we note that $h(\varepsilon)$ is given by,

$$h(\varepsilon) = \left(\frac{1-\varepsilon}{\varepsilon}\right) b \tag{9}$$

or in terms of ε, $\varepsilon = b/(b+h)$. From Eq. (7), the frictional drag force then becomes

$$F_d^{SH} = \frac{2}{3}\left[\frac{1+3\eta_{gl}F(\varepsilon)}{1+2\eta_{gl}F(\varepsilon)}\right] F_d^{St}(a) \tag{10}$$

where the superscript SH denotes a superhydrophobic surface. In our case, the comparison of drag forces is not between a compound droplet and a solid sphere both of radius a, but between a solid sphere of radius b and a plastron-retaining solid sphere of net radius $a=b+h$. Using Eq. (10), the correction factor, ξ_{SH}, for the drag force due to the presence of a concentric plastron is therefore,

$$\xi_{SH} = \frac{F_d^{SH}}{-6\pi\eta_l b U_\infty} = \frac{2}{3\varepsilon}\left[\frac{1+3\eta_{gl}F(\varepsilon)}{1+2\eta_{gl}F(\varepsilon)}\right] \tag{11}$$

The drag force correction depends on two dimensionless variables: h/b and η_{gl}. In drag experiments the measured quantity is often the coefficient of drag, C_D; for the plastron-retaining sphere, C_D can be written as,

$$C_D \equiv \frac{F_d}{\frac{1}{2}\rho_s U_\infty^2 \pi b^2} = \frac{24\xi_{SH}}{\mathrm{Re}} \tag{12}$$

where $Re=2\rho_s U_\infty b/\eta_l$ is the Reynolds number written in terms of the density, ρ_s, of the solid sphere.

i) Analytical Limits

The first limit we examine is that of a vanishing plastron with $h\to 0$, which corresponds to $\varepsilon\to 1$ and $b\to a$. Since $F(\varepsilon)\to\infty$ as $\varepsilon\to 1$, $\xi_{SH}\to 1$ from Eq. (11) and so we recover the usual Stokes drag for a solid sphere of radius b.[34] In this limit, it is important that the viscosity ratio, η_{gl}, of gas-to-liquid is not assumed zero even though it is small. The Stokes limit is approached from below and is only fully realized when the air circulation within the plastron is suppressed. Analytically, an expansion of Eq. (11) can be performed using h/b as the small parameter (which means $F(\varepsilon)^{-1}$ is also small) thereby yielding,

$$\xi_{SH} = \frac{1}{\varepsilon}\left[\frac{1+\dfrac{1}{3\eta_{gl}F(\varepsilon)}}{1+\dfrac{1}{2\eta_{gl}F(\varepsilon)}}\right] \to \frac{1}{\varepsilon}\left[1-\frac{1}{6\eta_{gl}F(\varepsilon)}\right] \approx 1-\left(\frac{1}{4\eta_{gl}}-1\right)\frac{h}{b}+\ldots \tag{13}$$

Provided $\eta_{gl}<1/4$, the first order correction for a plastron of thickness h causes a reduction of total drag compared to the same solid spherical object without a plastron.[35]

In the opposite limit of $h\to\infty$, the radius of the compound object is approximately h and since $F(0)\to 1/2$, Eq. (10) gives a drag force of,

$$F_d^{SH} = \frac{2}{3}\left[\frac{1+3\eta_{gl}/2}{1+\eta_{gl}}\right]F_d^{St}(h) \tag{14}$$

which is the Hadamard-Rybczynski result for a gas bubble.[26,30-32] Here ξ_{SH} increases proportional to $2(1+h/b)/3$ so that the drag is essentially that of a bubble of radius $b+h$. This drag clearly increases with the plastron thickness.

In light of the above results, there must exist for $\eta_{gl}<1/4$ an optimum plastron thickness, $h^* > 0$, for which the drag force is a minimum. When $h = h^*$, there is a balance between the reduction of drag associated with air circulation inside the plastron and the increase of drag associated with expanding the physical dimension of the compound object. Here, one can make a helpful analogy with a problem from heat transfer, namely the addition of insulating material to a body whose mean temperature is moderately larger, say, than that of the ambient. Such an addition of material reduces the thermal connectivity between the body and its surroundings but also increases the surface area

over which heat transfer may occur. If the layer is sufficiently thin, addition of insulation therefore increases, rather than decreases, heat loss from the convectively cooling body.[36]

ii) Numerical Calculations

To further elucidate how the drag of a plastron-retaining sphere depends on the thickness of the plastron, fig. 2 shows the Stokes drag correction factor, ξ_{SH}, as a function of normalized plastron thickness, h/b. Using the viscosity values at 20°C for air and water (i.e. $\eta_g=18.37\times10^{-6}$ kg m^{-1} s^{-1} and $\eta_l=1.002\times10^{-3}$ kg m^{-1} s^{-1}), the ratio of viscosities is $\eta_{gl}=0.0183$ and a minimum value of $\xi_{SH}=0.807$ is predicted to occur when $h/b=0.0835$. Thus, for a sphere of radius b, plastrons of uniform thicknesses $0.1b$ and $0.01b$ should reduce drag by around 19% and 8.7%, respectively.

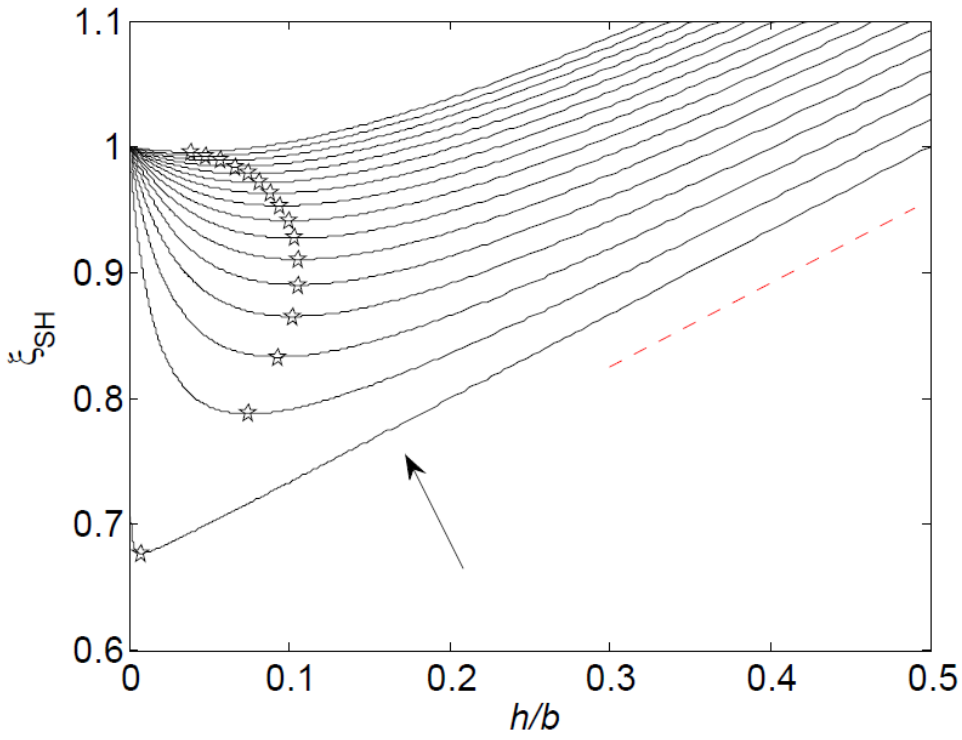

Figure 2. [Colour] Drag correction factor, ξ_{SH}, as function of normalized plastron thickness, h/b. The gas-to-liquid viscosity ratios are $\eta_{gl}=1\times10^{-4}$, $\eta_{gl}=1.34\times10^{-2}$, $\eta_{gl}=2.68\times10^{-2}$, ... $\eta_{gl}=0.187$, $\eta_{gl}=0.2$. The arrow shows the direction of increasing η_{gl}. Star symbols indicate the global minimum of each curve. The (red) dashed line has a slope of 2/3.

Corresponding to the above drag calculations, fig. 3 plots streamlines of the interior and exterior flow for values of plastron thickness below, above and at the optimum plastron thickness, h^*. When the plastron is extremely thin, the streamline pattern reproduces that expected for creeping flow around a sphere (fig. 3a). As the plastron thickness increases, an internal circulation of air within the plastron can be observed in a similar manner to that which occurs for a gas bubble retaining a non-rigid gas-liquid interface when immersed in a flowing liquid (fig. 3b, 3c). As the plastron increases further in thickness the cross-sectional area of the compound object becomes notably larger (fig. 3d). This sequence demonstrates the physical process leading to an initial reduction then progressive increase in drag as h grows in magnitude.

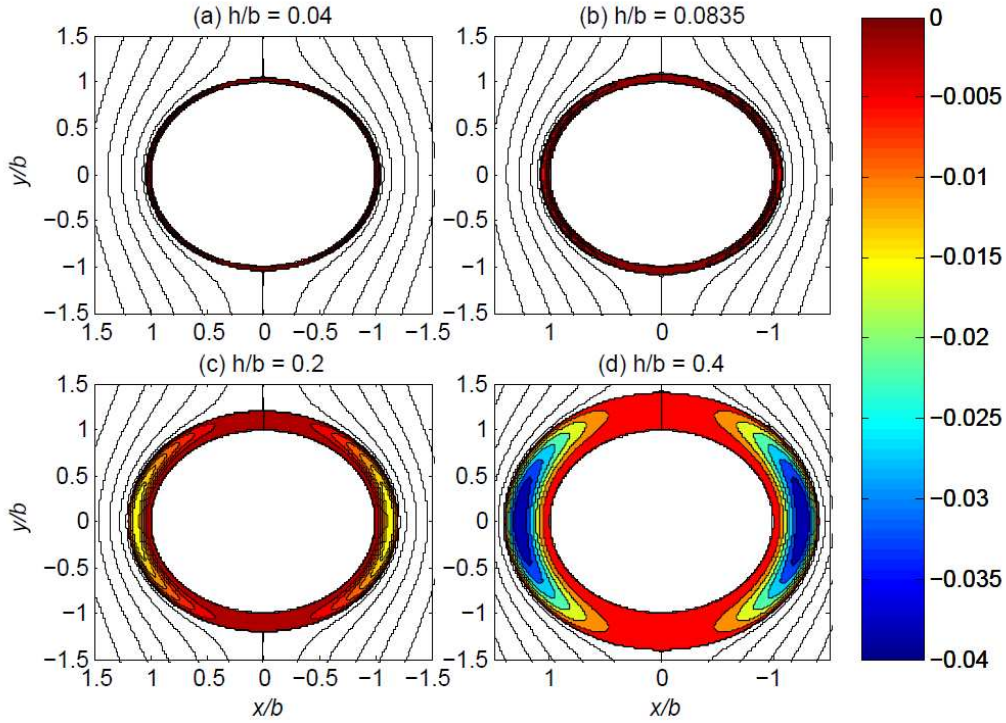

Figure 3. [Colour] Normalized streamline patterns around a plastron-retaining sphere for η_{gl}=0.0183 and various h/b including, in panel (b), the drag-minimizing optimum thickness h^*/b=0.0835. The streamline pattern within the plastron, i.e. $\psi_g/(U_\infty b^2)$, is shown with the colour contours. Outside of the plastron, streamlines are shown at $\psi_l/(U_\infty b^2)$=0.01, 0.04, 0.1, 0.175 and 0.3.

3.2 Apparent Slip

When there is no layer of air at the solid-liquid interface the usual boundary condition for a simple liquid, such as water, flowing past a smooth solid is the no-slip boundary condition. The concept of a slip boundary condition is that the extrapolation of the velocity profile of the flow in the external liquid, $u_r^l(r)$, to match that of the solid, $u_r^s(r)$, occurs at a location, say $r=b-l_s$, other than the physical interface, $r=b$, between the solid and the liquid. Using a Taylor series expansion, we write

$$u_r^s(b) = u_r^l(b-l_s) \approx u_r^l(b) - l_s\left(\frac{\partial u_r^l}{\partial r}\right)_{r=b} \tag{15}$$

where l_s, is the slip length. Eq. (15) allows the slip length to be defined in terms of the mismatch in velocities at the boundary and the shear stress (divided by the viscosity of the liquid η_l),[25]

$$l_s \approx \Delta u_r(b) \Big/ \left(\frac{\partial u_r^l}{\partial r}\right)_{r=b} \tag{16}$$

Often, a slip parameter or coefficient, $\beta_s=\eta_l/l_s$, is used in the literature since this is the ratio of the shear stress at the interface for a given velocity mismatch. If one believes the mismatch in velocities to represent a real effect, then the slip is termed real slip. However, a plastron interposed between a solid boundary and an external flow lubricates the flow and gives rise to an apparent slip. The

effect of the air layer is to replace the boundary condition for the external flow by a continuity of shear stress condition.

Basset[37] found that the drag force, F_d^s, on a solid sphere in a liquid subject to a slip boundary condition can be expressed as a correction to the Stokes drag assuming no-slip using,

$$\xi_{slip} = \frac{F_d^s}{-6\pi\eta_l b U_\infty} = \left[\frac{1+2\eta_l/\beta b}{1+3\eta_l/\beta b}\right] \tag{17}$$

Previous researchers have commented that the unbounded flow field caused by the migration of a slip solid sphere is the same as the external flow field generated by the same motion of a spherical fluid drop with a value of $\beta=3\eta_l/b$.[38,39] Thus, the slip length is one third of the radius of the sphere, i.e. $l_s=b/3$. With a plastron-bearing superhydrophobic solid sphere, however, this is not the correct physical situation: the solid core remains solid, but retains a layer of air of a finite thickness. We therefore expect the slip length to depend on the thickness of the plastron. Comparing Eq. (17) with Eq. (11) for the drag correction factor due to a plastron gives,

$$\beta = \frac{\eta_l}{b}\left[\frac{1+3\left(\frac{h}{b}\right)+\left(\frac{\eta_{lg}}{F(\varepsilon)}\right)\left(\frac{h}{b}\right)}{\left(\frac{1}{2}-\frac{h}{b}\right)\left(\frac{\eta_{lg}}{3F(\varepsilon)}\right)-\left(\frac{h}{b}\right)}\right] \tag{18}$$

The slip length is then given by,

$$l_s = b\left[\frac{\left(\frac{1}{2}-\frac{h}{b}\right)\left(\frac{\eta_{lg}}{3F(\varepsilon)}\right)-\left(\frac{h}{b}\right)}{1+3\left(\frac{h}{b}\right)+\left(\frac{\eta_{lg}}{F(\varepsilon)}\right)\left(\frac{h}{b}\right)}\right] \tag{19}$$

Using $\eta_{lg}=(\eta_{gl})^{-1}=54.5$, we note that the slip length becomes negative when $h/b > 0.454$. To the left of this point, l_s reaches a maximum value of $l_s/b=0.458$ at $h/b=0.0835$ at which point the drag is a global minimum (fig. 3b). For small h/b (i.e. up to 0.01), l_s is directly proportional to the plastron thickness. Analytically, Eq. (19) gives $l_s=(-1+\eta_{lg}/4)h$ demonstrating that the slip length can be an order of magnitude larger than the plastron thickness; this is consistent with the "order of magnitude" estimate given by Eq. (2.4) of Vinogradova.[40] The dependence of the slip length on the plastron thickness is shown in fig. 4.

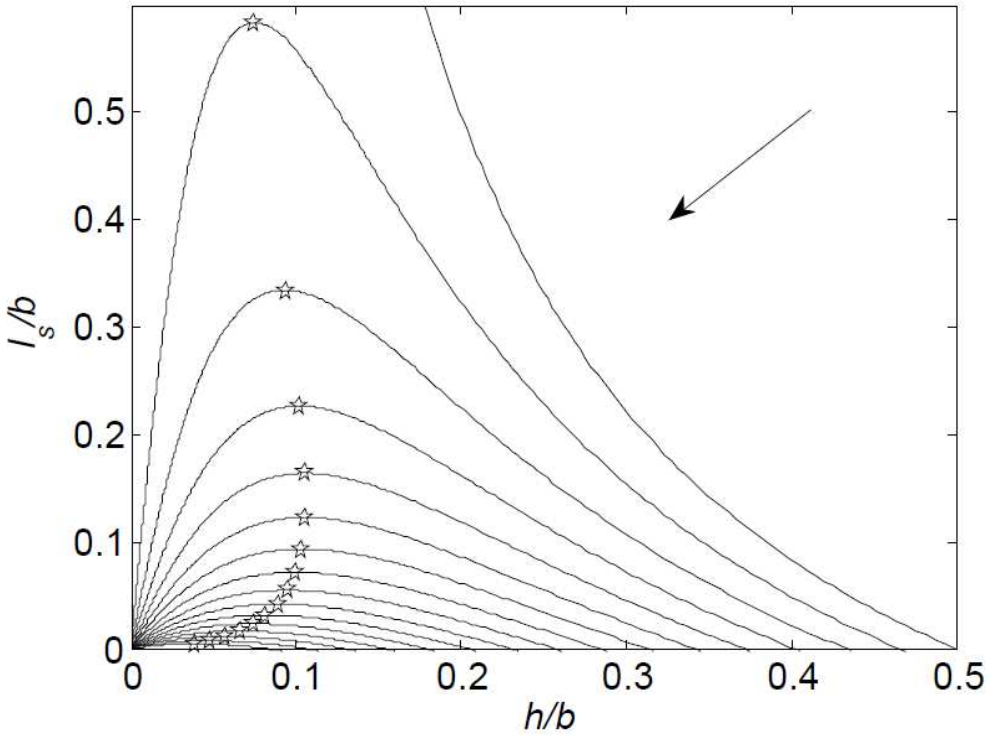

Figure 4. Normalized slip length, l_s/b, as a function of normalized plastron thickness, h/b, for the range of viscosity ratios indicated in figure 1. The arrow shows the direction of increasing η_{gl} (or decreasing η_{lg}). Star symbols indicate the global maximum of each curve.

3.3. Terminal Velocity

If a plastron-bearing superhydrophobic sphere is allowed to freely settle in a large volume of water containing no impurities or surfactants, the terminal velocity will, in general, differ from that for a smooth solid sphere of the same density and radius. At low *Re*, the two competing effects caused by the plastron will be the decrease in drag due to the drag correction factor ξ_{SH} and the increase in buoyancy due to the layer of air in the plastron.

At terminal velocity, the drag, buoyancy and gravitational forces must balance and consequently,

$$\xi_{SH} F_d^{St}(b) = \frac{-4\pi b^3 \left(\rho_s \varepsilon^3 + \left(1-\varepsilon^3\right)\rho_g - \rho_l\right) g}{3\varepsilon^3} \tag{20}$$

where ρ_s, ρ_l and ρ_g << ρ_s, ρ_l are the densities of the solid, air (gas) in the plastron and the water (liquid), and g=9.81 m s^{-2} is the acceleration due to gravity. Using Stokes' drag formula, $F_d^{St}(b) = -6\pi\eta_l b U_T^{SH}$, where U_T^{SH} denotes the terminal velocity, gives,

$$U_T^{SH} = \frac{2b^3 \left(\rho_s \varepsilon^3 + \left(1-\varepsilon^3\right)\rho_g - \rho_l\right) g}{9\varepsilon^3 \eta_l b \xi_{SH}} \tag{21}$$

which can be re-written as,

$$U_T^{SH} = \frac{U_T^{St}}{\xi_{SH}}\left[1 - \frac{\left(1-\varepsilon^3\right)}{\varepsilon^3}\frac{\Delta\rho_{lg}}{\Delta\rho_{sl}}\right] \tag{22}$$

where $\Delta\rho_{lg}=\rho_l-\rho_g$ and $\Delta\rho_{sl}=\rho_s-\rho_l$ and U_T^{St} is the terminal velocity given by Stokes' law for a solid sphere devoid of plastron. In the limit of a thin gas shell, $(1-\varepsilon^3)/\varepsilon^3 \approx 3h/b$, which becomes vanishingly small as $h \to 0$. Thus the correction factor for the terminal velocity is given by $1/\xi_{SH} \approx 1+(\eta_{lg}/4-1)h/b$; provided $\eta_{lg} > 4$ (i.e. $\eta_{gl} < 1/4$), drag reduction will outweigh the retarding effect associated with the buoyancy of the plastron. Conversely at large h, buoyancy dominates to the extent that the compound object rises rather than falls. Eq. (22) then recovers the known result for a bubble of gas rising at a terminal velocity dictated by the Hadamard-Rybczynski result. Correspondingly, we expect there to be a limited range of plastron thicknesses for which the terminal velocity, U_T^{SH}, exceeds the value predicted by Stokes' law and a unique thickness, h', for which U_T^{SH} is maximized. This prediction is corroborated by fig. 5, which shows solutions to Eq. (22) for various η_{gl} and two solid-to-liquid density ratios, $\rho_s/\rho_l = 2.5$ and $\rho_s/\rho_l = 5$.

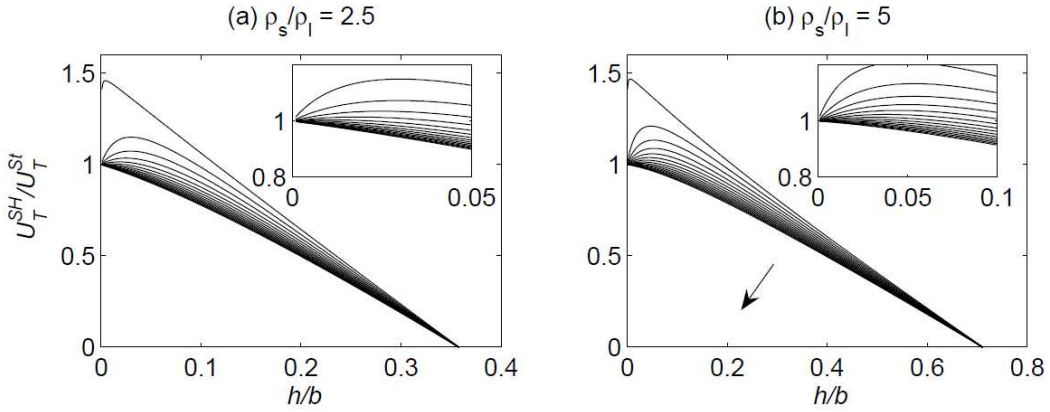

Figure 5. The effect on the terminal velocity of a settling sphere carrying a plastron (i.e. U_T^{SH}/U_T^{St}) as a function of plastron normalized thickness, h/b, for the range of viscosity ratios indicated in figure 1. The arrow shows the direction of increasing η_{gl}. (a) ρ_s/ρ_l=2.5, and (b) ρ_s/ρ_l =5. In either case, the inset shows the behaviour for small h/b and U_T^{SH}/U_T^{St} close to unity. In the special circumstance h/b=0, U_T^{SH}/U_T^{St}=1 for all η_{gl}, i.e. the limit prescribed by Stokes' law is recovered.

The insets to fig. 5 make clear that h' is a function both of η_{lg} and ρ_s/ρ_l. This dependence contrasts with the drag reduction of fig. 2 and slip length of fig. 4, neither of which vary with the density ratio, and which therefore have extrema (given by the star symbols) at identical values of h/b. From the pre-factor ξ_{SH}^{-1} on the right-hand side of Eq. (22), it is evident that the point of maximum drag reduction will coincide with the point of maximum terminal velocity when the density of the solid is much larger than that of the liquid, and hence also of the gas. Physically, the buoyancy of the plastron is irrelevant in this case owing to the very large density of the solid. A similar coincidence is anticipated when η_{gl}=0. By contrast, under less extreme circumstances (i.e. $\rho_s < \infty$, $\eta_{gl}>0$), we expect h^* and h' to differ and, more specifically, that $h^*>h'$. Both of these predictions are indicated in fig. 6, which shows h^*/b and h'/b as functions of the density ratio ρ_s/ρ_l and the viscosity ratio η_{gl}. Consistent with figs. 2 and 4, h^*/b is independent of ρ_s/ρ_l and is,

moreover, first an increasing then a decreasing function of η_{gl}. On the other hand, and further to fig. 5, h'/b depends both upon the density and viscosity ratios. The qualitative variation of h'/b on η_{gl} is similar to that associated with h^*/b. Conversely h'/b is a monotonically increasing function of ρ_s/ρ_l, which again reflects the fact that thicker plastrons can be accommodated when the solid density, ρ_s, is large.

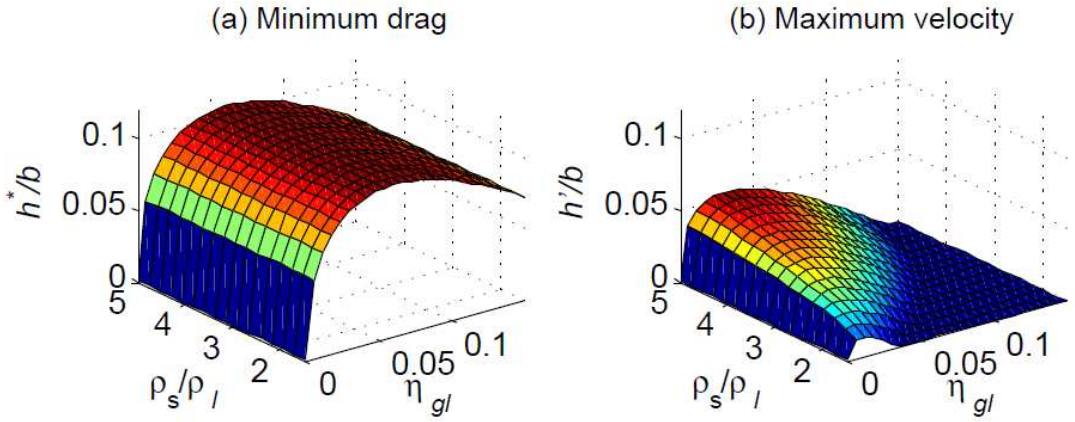

Figure 6. [Colour] Optimum plastron thickness as a function of ρ_s/ρ_l and η_{gl}. In (a), h^*/b corresponds to the plastron-retaining sphere having the minimum drag. In (b), h'/b corresponds to the plastron-retaining sphere having the maximum terminal velocity.

4. Discussion

The present analysis examines a model of a perfect superhydrophobic surface, namely a solid sphere that is encased within a sheathing plastron of uniform thickness. Within the context of this idealized model, it is assumed that the influence of surface tension outweighs that of viscosity so that the air-water interface does not deform.[28] As discussed in the introduction, in a plastron the interface is effectively stiffened and maintained at a constant thickness due to the hydrophobic surface structure supporting and maintaining the gas layer. We assume, moreover, that conditions are such that the interior and exterior flows are described by Stokes' flow. Formally, our analysis is restricted to the small capillary and Reynolds numbers regimes i.e. $Ca<0.5$, $Re<<1$.

Of course, the ability of a superhydrophobic surface to retain an encapsulating air layer depends in part on surface chemistry but also on the details of the surface topography; for long term effectiveness in drag reduction the air layer also needs to be persistent.[41] In the case of aquatic or semi-aquatic insects, for example, the integument often consists of a dense array of long, waxy hairs, which are bent near the tip and therefore take the shape of an inverted 'L' (see figs. 6, 10 and 11 of Thorpe[6] or fig. 3 of Flynn and Bush[9]). By contrast, biomimetic engineered surfaces are typically characterized by a regular array of indentations and/or protrusions.[42] In either circumstance, the presence of these micro-scale features is expected to depress air velocities within the plastron due to the additional viscous drag associated with flow past this micro-topography. So whereas the curves of figure 2 exhibit unambiguous minima corresponding to the smallest possible drag experienced by a plastron-retaining superhydrophobic sphere, the associated predictions of $(\xi_{SH})_{\min}$ and h^*/b may be conservative.

In extreme cases, e.g. meridionally-aligned ridges covering the surface of a superhydrophobic sphere, the scale of the air circulation cells may be dictated by the ridge-spacing rather than the sphere diameter. Such is the case in the numerical study of Gao and Feng[25], who studied flow over a superhydrophobic surface that is comprised of a series of posts with non-penetrating liquid bridging between adjacent posts and thus consists of a periodic surface with a set of air bubbles within the surface structure. Gao and Feng[25] found that air circulation cells develop within each bubble, which are qualitatively similar to the larger cells exhibited in figure 3. Indeed they argued that depinning of the contact lines around each bubble can promote the formation of a continuous layer of air. Whilst we are unaware of any solutions to the equations of Rushton and Davies[27] that are not of the form exhibited in figure 3, Gao and Feng's numerical results suggest it should be possible to extend the approach in our work to a series of connected air volumes co-located on the solid hydrophobic surface. In the limiting case, isolated bubbles of the type examined in a different context by Sugiyama and Sbragaglia[24] are expected. From the analysis of Gao and Feng,[25] it is known that the relationship between drag and circulation cell size is a sensitive function of the fraction of exposed solid surface, at least in the Cartesian geometry examined in their investigation. However, for the regime of interest here where surface tension dominates over viscosity (and inertia is negligible), their figs. 9 and 10a suggest that the drag is essentially independent of cell size.

The above considerations add extra constraints in the context of superhydrophobic material design and fabrication: adjacent surface topographic elements must be positioned close enough to maintain the integrity of the plastron but not in such an orientation as to stifle zonal air flow or with a symmetry or density that impedes the connectivity of the space. Although quantifying these geometric considerations for a particular application remains the topic of on-going research, it should be recalled that reproducible drag reduction was measured in recent experiments in which solid spheres were coated with a random array of hydrophobic sand grains.[21] An important point of difference between these experiments and the theory described above is the relatively large Reynolds number (i.e. $Re \sim 1\times10^4$ to 3×10^4) applied in the former. In this inertia-dominated regime, interface rigidification by surfactant accumulation is expected to be negligible and, more significantly, flow separation is anticipated in the lee of the sphere. A thick plastron can be expected to modify the separation points[3,21] and/or wake cross-sectional area[43] and thereby depress the drag in greater proportion than is reported in fig. 2 above, which considers the Stokes limit $Re<<1$.[#] Indeed, this effect that has recently been reported using a terminal velocity experiment with a solid sphere retaining a Leidenfrost induced vapour layer.[22] The fact that McHale *et al.*'s experiments employed irregular hydrophobic surfaces suggests that nontrivial drag reduction can be achieved even for non-optimized surface topography.

Returning briefly to the natural world, not all aquatic and semi-aquatic arthropods use their plastron for respiratory purposes. A case in point is the 1.5 mm long intertidal midge *Clunio*, which was the topic of a recent theoretical and experimental investigation by Neumann and Woermann[23]. They remark that, upon submersion, "parts of their bodies are covered by a thin layer of air, other parts are surrounded by [a thick] air bubble located between body and extremities" (see their fig. 1). The function of the plastron is to protect *Clunio* "against shearing forces which otherwise could injure the insect's extremities during submersion in the churning sea." Such protection would be

[#] Note added to postprint: See also P. Muralidhar, N. Ferrer, R. Daniello and J.P. Rothstein, *J. Fluid Mech*. **2011**, *680*, 459-476.

especially substantial in the case of a surfactant-rigidified air-water interface, although ocean turbulence could then transport the plastron-retaining insect longer distances than would be the case for a clean, free-slip interface. Neumann and Woermann[23] further remark that *Clunio* specimens adhered to the inner surface of the (glass) container in which they were submerged in the laboratory. To the limited extent that *Clunio* may be able to adhere to rocky substrate when struck by an incoming wave or its spray, the presence of an encapsulating air bubble will reduce the drag forces experienced by the insect and thereby decrease the likelihood of it being washed away.

Biological plastrons are not limited to the adult stage of development, but appear also in insect eggs, particularly terrestrial eggs laid in environments subject to occasional flooding.[44,45] Egg plastrons fill the chorionic void spaces and also appear along the chorion surface yielding a silvery sheen, e.g. along the dorsal side of blow-fly eggs.[46] Although the respiratory function of these plastrons is well-established, there is also the possibility that they serve a drag-reducing role. To our best knowledge, this alternative has not been previously considered and will comprise the topic of a future investigation. Likewise, we intend to investigate the possibility that the air circulation cells depicted in figure 3 enhance the transport of oxygen and carbon dioxide within insect and insect egg plastrons. If this conjecture is valid, it suggests, for example, that the spacing between adjacent breathing tubes in insect integument, and indeed the scale of the plastron, is not dictated solely by molecular diffusion.

5. Conclusion

In this work drag reduction at low Reynolds numbers for a superhydrophobic sphere has been considered using a simple analytical model of a continuous sheathing plastron. It has been shown that significant (i.e. 20 to 30%) reductions in drag are possible due to the induced internal circulation of the gas within the plastron. The presence of a plastron results in a competition between drag reduction from the internal gas circulation and drag increase from expanding the effective cross-sectional area of the compound object. This competition yields an optimum plastron thickness, h^*, for drag reduction. The overall drag reduction is sufficiently large that in the context of a solid sphere settling in water under gravity, it can outweigh the effect of the increased buoyancy from the air in the plastron. At small plastron thicknesses, the drag reduction can be equated to an effective slip length and, for an air-water system, this slip length is an order of magnitude larger than the plastron thickness, which itself is set by the size of the topographic features. Our results can thereby guide the design of drag-reducing superhydrophobic surfaces; they suggest, for instance, that topographic features should be large enough to provide an optimum thickness plastron, yet designed and distributed such that circulation within the plastron is not suppressed. Finally, the relevance of this model to intermediate and high Reynolds number flows and to the possibility that some insect plastrons fulfil a drag reduction role, rather than just a respiration role, are discussed.

Acknowledgements

The authors' acknowledge financial assistance from the U.K. Engineering and Physical Sciences Research Council (Grant Nos. EP/E063489/1 and EP/G057265/1) and the Canadian Natural Science and Engineering Research Council (Discovery Grant program). GM and MIN would like to acknowledge discussions with A. Busse, I. Campbell, B. Gruncell, N.D. Sandham and S. Stanley.

References

1. D. Quéré, *Annu. Rev. Mater. Res.*, 2008, **38**, 71–99.
2. P. Roach, N. J. Shirtcliffe and M. I. Newton, *Soft Matter*, **2008**, *4*, 224-240.
3. G. McHale, M. I. Newton and N. J. Shirtcliffe, *Soft Matter*, **2010**, *6*, 714-719.
4. D. J. Crisp and W. H. Thorpe, *Trans. Farad. Soc*., **1948**, *44*, 210-220; 270-303.
5. W. H. Thorpe and D. J. Crisp, *J. Exp. Biol.*, **1947**, *24*, 227-269.
6. W. H. Thorpe, *Biol. Rev.*, **1950**, *25*, 344-390.
7. J. Scott-Turner, 2000. The Extended Organism: The Physiology of Animal-Built Structures, Harvard University Press, Cambridge, Massachusetts and London, England. Chapter 8.
8. N. J. Shirtcliffe, G. McHale, M. I. Newton, C. C. Perry and F. B. Pyatt, *Appl. Phys. Lett.* **2006**, *89*, art 104106.
9. M. R. Flynn and J. W. M. Bush, *J. Fluid Mech*., **2008**, *608*, 275-296.
10. J. P. Rothstein, *Annu. Rev. Fluid Mech.*, **2010**, *42*, 89-109.
11. R. S. Voronov, D. V. Papavassiliou and L. L. Lee, *Ind. Engn. Chem. Res*., **2008**, *47*, 2455-2477.
12. D. Quéré, A. Lafuma and J. Bico, *Nanotechnology*, **2003**, *14*, 1109-1112.
13. J. Ou and J. P. Rothstein, *Phys. Fluids*, **2005**, *17*, art. 103606.
14. P. Joseph, C. Cottin-Bizonne, J. M. Benoit, C. Ybert, C. Journet, P. Tabeling and L. Bocquet, *Phys. Rev. Lett*., **2006**, *97*, art. 156104.
15. S. Gogte, P. Vorobieff, R. Truesdell, A. Mammoli, F. van Swol, P. Shah and C.J. Brinker, *Phys. Fluids*, **2005**, *17*, art. 051701.
16. C. H. Choi and C. J. Kim, *Phys. Rev. Lett.*, **2006**, *96*, art. 066001.
17. N. J. Shirtcliffe, G. McHale, M. I. Newton and Y. Zhang, *ACS Appl. Mater. Interf.* **2009**, *1*, 1316-1323.
18. P. Roach , G. McHale G, C. R. Evans, N. J. Shirtcliffe and M. I. Newton, *Langmuir*, **2007**, *23*, 9823-9830.
19. M. Fujita, H. Muramatsu and M. Fujihira, M. *Japn. J. Appl. Phys*., **2005**, *44*, 6726-6730.
20. S. J. Kwoun, R. M. Lec, R. A. Cairncross, P. Shah and C. J. Brinker, *IEEE Trans. Ultrason. Ferroelectr. Freq. Control*, **2006**, *53*, 1400-1403.
21. G. McHale, N.J. Shirtcliffe, C. R. Evans and M. I. Newton, *Appl. Phys. Lett.* **2009**, *94*, art. 064104.
22. I. Vakarelski, J. Marston, D. Chan, and S. Thoroddsen, *Phys. Rev. Lett.* **2011**, *106*, art. 214501.
23. D. Neumann and D. Woermann, *Naturwissenschaften*, **2009**, *96*, 933-941.
24. K. Sugiyama and M. Sbragaglia, *J. Eng. Math*. **2008**, *62*, 35-50.
25. P. Gao and J. J. Feng, *Phys. Fluids*, **2009**, *21*, 102102.
26. L. D. Landau and E. M. Lifshitz, **1959**. Fluid Mechanics, Pergamon Press, London.
27. E. Rushton and G. A. Davies, *Int. J. Multiph. Flow* **1983**, *9*, 337-342.
28. R.E. Johnson and S.S. Sadhal, *Ann. Rev. Fluid. Mech.* **1985**, *1*, 289-320.
29. J. M. Ferreira, A. A. Soares and R. P. Chhabra, *Fluid Dyn. Res*., **2003**, *32*, 210-215.
30. J.S. Hadamard, *C. R. Hebd. Séanc. Acad. Sci. (Paris)* **1911**, *152*, 1735-1738.
31. M.W. De Rybczynski, *Bull. Acad. Sci. Cracovie Ser. A* **1911**, 40-46.
32. J.C. Boussinesq, *C. R. Hebd. Séanc. Acad. Sci. (Paris)* **1913**, *156*, 983-989.
33. C. Priest, T. W. J. Albrecht, R. Sedev and J. Ralston, *Langmuir*, **2009**, *25*, 5655-5660.
34. G. G. Stokes, *Trans. Camb. Phil. Soc.* **1851**, *9*, 8-106.
35. R. E. Johnson, *J. Fluid Mech*., **1981**, *110*, 217-238.

36. F.P. Incropera and D. P. DeWitt, **1996**. Introduction to Heat Transfer, 3rd Edition, John Wiley and Sons, New York.
37. A. B. Basset, **1961**. In: A Treatise on Hydrodynamics, vol. 2. Dover, New York.
38. H. J. Keh and S. H. Chen, *Eur. J. Mech. B,* **1996** *15*, 791-807.
39. S. Senchenko and H. J. Keh, *Phys. Fluids* **2006** *18*, art. 088104.
40. O. I. Vinogradova, *Int. J. Miner. Proc.*, **1999**, *56*, 31-60.
41. A. Balmert, H. F, Bohn, P. Ditsche-Kuru and W. Barthlott, *J. Morph.*, **2011**, *272*, 442-451.
42. L. Cao, H.-H. Hu and D. Gao, *Langmuir*, **2007**, *23*, 4310-4314.
43. B. Gruncell and I. Campbell, University of Southampton, personal communication.
44. H.E. Hinton, *Ann. Rev. Entomol.*, **1969**, *14*, 343-368.
45. H.E. Hinton, *Nature*, **1959**, *184*, 280-281.
46. D. J. Crisp, **1964**. In: Recent Progress in Surface Science, vol. 2, Academic Press, New York.

Appendix A – Streamfunctions

Ferreira *et al.* give the streamfunction solutions for single and multiple compound droplets in a creeping flow regime.[1] For a fluid-encapsulated fluid core of radius b, in axisymmetric creeping flow the three stream functions are,

Core ($0 \le r \le b$)

$$\psi_3 = \frac{U_\infty r^2 \sin^2\theta}{2}\left(\frac{\eta_{12}\tilde{S}}{\tilde{\Delta}}\right)\left(1-\frac{r^2}{b^2}\right) \tag{A1}$$

where $\varepsilon = b/a$ and a is the radius of the fluid core together with the encapsulating fluid (see fig. 1 of the manuscript). Here U_∞ is the free stream velocity at large r and $\eta_{12} = \eta_1/\eta_2$ is the ratio of the viscosity of the sheathing fluid (phase 1) to the external fluid (phase 2).

Sheathing fluid ($b \le r \le b/\varepsilon$)

$$\psi_1 = \frac{U_\infty r^2 \sin^2\theta}{2}\left(\frac{1}{1-\varepsilon^5}\right)\left(\frac{G(\varepsilon)}{\tilde{\Delta}}\right)\left[2\eta_{12}\left(\frac{\varepsilon^2 r^2}{b^2} - T + \frac{Tb}{r} - \frac{\varepsilon^2 b^3}{r^3}\right) + \eta_{32}(1-\varepsilon)\left(\frac{\tilde{U}\varepsilon^2 r^2}{b^2} - \tilde{V} + \frac{\tilde{W}b}{\varepsilon r} - \frac{\tilde{X}b^3}{r^3}\right)\right] \tag{A2}$$

where $\eta_{32} = \eta_3/\eta_2$ is the ratio of the viscosity of the core fluid (phase 3) to the external fluid (phase 2).

External fluid ($b/\varepsilon \le r$)

$$\psi_2 = \frac{U_\infty r\left(r-\frac{b}{\varepsilon}\right)\sin^2\theta}{2}\left(\frac{1}{\tilde{\Delta}}\right)\left[2\eta_{12}F(\varepsilon) + \eta_{32} + \eta_{12}\left(2\eta_{12}G(\varepsilon) + \eta_{32}F(\varepsilon)\right)\left(1-\frac{b}{\varepsilon r}\right)\left(2+\frac{b}{\varepsilon r}\right)\right] \tag{A3}$$

where

$$\tilde{\Delta} = \eta_{32} + 4\eta_{12}^2 G(\varepsilon) + 2\eta_{12}(1+\eta_{32})F(\varepsilon) \tag{A4}$$

and

$$\tilde{S} = \frac{(\varepsilon^2 + 3\varepsilon + 1)}{(1-\varepsilon)(4\varepsilon^2 + 7\varepsilon + 4)} \tag{A5a}$$

$$T = \frac{(1-\varepsilon^5)}{(1-\varepsilon)} = \varepsilon^4 + \varepsilon^3 + \varepsilon^2 + \varepsilon + 1 \tag{A5b}$$

$$\tilde{U} = (\varepsilon + 2) \tag{A5c}$$

$$\tilde{V} = (3\varepsilon^3 + 6\varepsilon^2 + 4\varepsilon + 2) \tag{A5d}$$

$$\tilde{W} = \varepsilon(2\varepsilon^3 + 4\varepsilon^2 + 6\varepsilon + 3) \tag{A5e}$$

$$\tilde{X} = (2\varepsilon + 1) \tag{A5f}$$

In the limit of a solid core (i.e. $\eta_{32}\to\infty$), these equations reduce to,

$$\psi_3 = 0 \qquad 0 \le r \le b \tag{A6}$$

$$\psi_1 = \frac{U_\infty r^2 \sin^2\theta}{2}\frac{G(\varepsilon)}{1+2\eta_{12}F(\varepsilon)}\left(\frac{1}{T}\right)\left[\frac{\tilde{U}\varepsilon^2 r^2}{b^2} - \tilde{V} + \frac{\tilde{W}b}{\varepsilon r} - \frac{\tilde{X}b^3}{r^3}\right] \qquad b \le r \le b/\varepsilon \tag{A7}$$

$$\psi_2 = \frac{U_\infty r\left(r-\frac{b}{\varepsilon}\right)\sin^2\theta}{2}\left(\frac{1}{1+2\eta_{12}F(\varepsilon)}\right)\left[1+\eta_{12}\left(1-\frac{b}{\varepsilon r}\right)\left(2+\frac{b}{\varepsilon r}\right)F(\varepsilon)\right] \qquad b/\varepsilon \le r \tag{A8}$$

Note that ψ_1 vanishes at both b and b/ε, and ψ_2 vanishes at b/ε (see fig. 3 of the manuscript). In the limit $r\to\infty$, the stream function $\psi_2\to 0.5U_\infty r^2\sin^2\theta$, which is the expected free stream value.

Reference

1. J. M. Ferreira, A. A. Soares and R. P. Chhabra, *Fluid Dyn. Res.*, **2003** *32*, 210-215.